Estimation of carbon fluxes from eddy covariance data and satellite-derived vegetation indices in a karst grassland (Podgorski Kras, Slovenia)

Koffi Dodji Noumonvi

Dissertation to obtain a Master's Degree in

Mediterranean Forestry and Natural Resources Management (MEDfOR)

Supervisors: Dr. Sofia Cerasoli (Centro de Estudos Florestais)
Dr. Mitja Ferlan (Slovenian Forestry Institute)

Jury:
President: - Doutor Pedro César Ochôa de Carvalho, Professor Auxiliar do Instituto Superior de Agronomia da Universidade de Lisboa.

Members: - Doutor João Manuel das Neves Silva, Investigador Integrado da Fundação para a Ciência e aTecnologia;
- Doutora Sofia Cerasoli, Investigadora.

2018

Acknowledgements

First of all, I would like to thank God for helping me throughout this important step in my life.

I would like to express my sincere gratitude to Sofia Cerasoli and Mitja Ferlan for their very good supervision and support all the way. I thank them for contributing greatly to reach this quality of the dissertation.

I am also very thankful to the president of jury Prof. Pedro Ochôa and the jury member João Silva for their assessment of the document, and their valuable comments.

I am really grateful to the MEDfOR commission and the Education, Audiovisual and Culture Executive Agency (EACEA) of the European Union for this opportunity to study in some top universities in Europe.

Finally, I would like to thank my family and friends for their unfailing support so that whenever I felt down, I had someone to turn to.

Abstract

The Eddy covariance method is a widespread method used for measuring carbon fluxes between the atmosphere and the ecosystem. It provides a high temporal resolution of measurements, but it is restricted to an area around the tower called footprint, and other methods are usually used in combination with eddy covariance data in order to estimate carbon fluxes for larger areas. Spectral vegetation indices derived from increasingly available satellite data can be combined with eddy covariance data to estimate carbon fluxes outside of the tower footprint. Following that approach, the present study attempted to model carbon fluxes for a karst grassland in Slovenia. Three types of model were considered: (1) a linear relationship between NEE or GPP and each vegetation index, (2) a linear relationship between GPP and the product of a vegetation index with PAR, and (3) a simplified LUE model assuming a constant LUE. We compared the performance of several vegetation indices from two sources (Landsat and SPOT-Vegetation) as predictors of NEE and GPP, based on three accuracy metrics (R^2, RMSE and AIC). Two types of aggregation of flux data were explored, midday average fluxes and daily average fluxes. The Vapor Pressure Deficit was used to separate the growing season in two phases, a greening phase and a dry phase, which were considered separately in the modelling process, in addition to the growing season as a whole. The results showed that NDVI was the best predictor of GPP and NEE during the greening phase, whereas water related vegetation indices, namely LSWI and MNDWI were the best predictors during the dry phase, both for midday and daily aggregates. Model type 1 (linear relationship) was found to be the best in many cases. The best regression equations obtained were used to illustrate the mapping of GPP and NEE for the study area.

Keywords: Eddy covariance, carbon flux, GPP, NEE, Vegetation indices.

Resumo

O método micrometeorológico da covariância turbulenta é o método líder para medir as trocas de carbono entre a atmosfera e a biosfera. Apesar da alta resolução temporal destas medições, a área de influência é restrita ao redor da torre onde as medições são efectuadas. Os Índices de vegetação espectrais podem ser combinados com dados de covariância turbulenta para extender a estimativa dos fluxos de carbono para além da área de influencia da torre. Seguindo essa abordagem, o presente estudo tentou modelar os fluxos de carbono para uma pastagem cársica na Eslovênia. Três tipos de modelos foram considerados: (1) uma relação linear entre a Produtividade Primaria Liquida (PPL) ou a Produtividade Primária Bruta (PPB) e cada índice de vegetação, (2) uma relação linear entre PPB e o produto de um índice de vegetação com a radiação fotossinteticamente ativa e (3) um modelo simplificado de eficiência de uso de luz (EUL) no qual a EUL foi assumido como sendo constante. Comparamos o desempenho de vários índices de vegetação de duas fontes como preditores de PPL e PPB, com base em três métricas de exatidão (R^2, RMSE e AIC). Dois tipos de agregação de dados de fluxo foram explorados, a média dos fluxos por volta do meio dia solar e a média diária. O Défice de Pressão de Vapor foi utilizado para separar duas fases, ao longo do ano, uma fase de crescimento e uma fase de stress estival, que foram consideradas separadamente no processo de modelação. Os resultados mostraram que o NDVI foi o melhor preditor de PPB e PPL durante a fase de crescimento, enquanto os índices de vegetação relacionados com o conteúdo hidrico, LSWI e MNDWI foram os melhores preditores durante a fase de stress estival, tanto para o meio-dia como para os agregados diários. O modelo 1 foi o melhor em muitos casos. As melhores equações de regressão obtidas foram utilizadas para ilustrar o mapeamento de PPB e PPL para a área de estudo.

Palavras-chave: Método micrometeorológico da covariância turbulenta, Fluxo de carbono, PPB, PPL, Índices de vegetação.

Resumo alargado

As pastagens são um dos tipos de vegetação mais difundidos em todo o mundo. O fato de poderem atuar como fonte de carbono durante os eventos de seca levou a um fraco reconhecimento de seu papel no ciclo global de carbono. No entanto, as pastagens desempenham um papel considerável neste ciclo, uma vez que armazenam uma quantidade importante de carbono nos seus solos. Portanto, é importante estudar o sequestro de carbono nas pastagens e perceber de que maneira estas podem contribuir para mitigar os efeitos das mudanças climáticas. O método micrometeorológico da covariância turbulenta (eddy covariance) é a técnica líder mundial para medição das trocas de CO_2, H_2O e energia entre a biosfera e a atmosfera. O método tem a vantagem de realizar medições diretas de diferentes gáses com alta precisão e detalhes. A fim de monitorizar os fluxos de CO_2 e H_2O em pastagens , uma torre para a medição de fluxos pelo método da covariância turbulenta foi instalada na regiaõ de Podgorski Kras desde 2008, fornecendo medições da Produtividade Primaria Liquida (PPL) e da evapotranspiração. Apesar da alta resolução temporal destas medições, a área de medição é restrita a uma área de influência ao redor da torre, com um alcance de cerca 200m.

Os índices de vegetação espectral derivados de dados de satélite podem ser combinados com dados obtidos por meio da covariância turbulenta, para estimar os fluxos de carbono para além da area de influencia da torre. Diferentes tipos de modelos matemáticos existem para este fim. Estes são baseados no conceito simples, mas eficaz, de eficiência de uso de luz (EUL) de Monteith, que está enraizado na forte relação existente entre a Produtividade Primária Bruta (PPB) e a radiação fotossinteticamente ativa (RFA) absorvida pela vegetação. No entanto, esse tipo de modelo mostrou-se frequentemente limitado, devido à dificuldade em determinar alguns de seus parâmetros. Como alternativa, alguns estudos estimaram PPB ou PPL por meio de regressão linear, adotando índices espectrais de vegetação como variáveis explicativas.

Reunindo dados de covariância turbulenta e índices de vegetação, o presente estudo tentou modelar fluxos de carbono para a pastagem Cársico Eslovena. Três tipos de modelos foram considerados: (1) uma relação linear entre PPL ou PPB e cada índice de vegetação, (2) uma relação linear entre PPB e o produto de um índice de vegetação com RFA e (3) um modelo simplificado de eficiência de uso de luz no qual EUL foi assumido como sendo constante. Comparamos o desempenho de vários índices de vegetação de duas fontes (Landsat e SPOT-Vegetation) como preditores de PPL e PPB, com base em três métricas de exatidão (R^2, RMSE e AIC). Dois tipos de agregação de dados de fluxo foram explorados, a média dos fluxos por volta do meio dia solar e a média diária. O Déficit de Pressão de Vapor foi utilizado para separar duas fases, ao longo do ano, uma fase de crescimento e uma fase de stress estival, que foram consideradas separadamente no processo de modelação. Os resultados foram comparados com as regressões obtidas considerando uma única estação de crescimento.

Os resultados mostraram que o NDVI foi o melhor preditor de PPB e PPL durante a fase de crescimento, enquanto os índices de vegetação relacionados com o conteúdo hidrico, LSWI e MNDWI foram os

melhores preditores durante a fase de stress estival, tanto para o meio-dia como para os agregados diários. Embora os resultados das duas fontes de índices de vegetação não pudessem ser comparados, observamos que os R^2 obtidos a partir dos NDVIs (NDVI da SPOT-Vegetation) foram geralmente menores do que o R^2 obtido a partir dos índices de vegetação derivados de Landsat. No geral, os fluxos médios do meio-dia estavam mais correlacionados com os índices de vegetação do que os fluxos médios diários. Isto deve-se a uma menor flutuação nos fluxos médios do meio-dia devido à reduzida escala de tempo considerada. O modelo tipo 1 (relação linear entre fluxos e índices de vegetação) foi o melhor em muitos casos, confirmando o fato de que a radiação fotossinteticamente ativa absorvida (RFAA) pela vegtação, ou seja a área foliar explica a maior parte da variabilidade de PPB em um ecossistema caracterizado por uma marcada sazonalidade como pastagens e culturas agrícolas anuais. As melhores equações de regressão obtidas foram utilizadas para ilustrar o mapeamento de PPB e PPL para a área de estudo. Mapas de fluxos de carbono ajudam a avaliar sua variabilidade espacial e temporal. O índice NDVI, independentemente do satellite utilizado, mostrou na maioria dos casos distribuições similares, com diferenças causadas principalmente pela diferença na resolução espacial.

Uma das principais limitações deste estudo é o fato de que não houve validação dos melhores modelos selecionados devido a uma quantidade limitada de dados disponiveis. Além disso, o fato de obter melhores resultados separando o ciclo anual em duas fases climáticas sugere que o uso dos resultados em grandes áreas vai necessitar de dados climáticos para o calculo de VPD (por exemplo, de estações meteorológica). A adoção de regressões empíricas restringe a utilidade dos modelos para áreas com condições semelhantes. Recomendações para pesquisas futuras seriam a validação dos modelos, assim que os dados estivessem disponíveis. As imagens do Landsat 7 também podem ser exploradas para usar todos os dados de covariância turbulenta disponíveis antes de 2014.

Palavras-chave: Método micrometeorológico da covariância turbulenta, Fluxo de carbono, PPB, PPL, Índices de vegetação.

Table of content

List of Figures

List of Tables

List of Abbreviations

AIC: Akaike Information Criterion

APAR: Absorbed Photosynthetically Active Radiation

EC: Eddy Covariance

EVI: Enhanced Vegetation Index

fAPAR: Fraction of Absorbed Photosynthetically Active Radiation

GNDVI: Green Normalized Difference Vegetation Index

GPP: Gross Primary Productivity

LSWI: Land Surface Water Index

LUE: Light Use Efficiency

LUE_{max}: Maximum Light Use Efficiency

MNDWI: Modified Normalized Difference Water Index

NDSVI: Normalized Difference Senescent Vegetation Index

NDVI: Normalized Difference Vegetation Index

NDVIs: Normalized Difference Vegetation Index from SPOT-Vegetation mission

NEE: Net Ecosystem Exchange

P: Precipitation

r: Pearson Correlation Coefficient

R^2: Coefficient of determination

R_{eco}: Respiration of the Ecosystem

RMSE: Root Mean Square Error

SAVI: Soil Adjusted Vegetation Index

SWC: Soil Water Content

Tair: Air Temperature

VI: Vegetation Index

VPD: Vapor Pressure Deficit

1. Introduction

Grasslands are one of the most widespread vegetation types worldwide, covering between 14 and 26% of the earth surface (Mason and Zanner, 2005; Scurlock and Hall, 1998). Moreover, they are increasing in area recently due to the abandonment of former agriculture lands in some parts of the world. In fact, the transformation of the agricultural context has released many areas from use in Europe, and such areas would naturally undergo succession (Benjamin et al., 2005) from grasslands to shrublands and forests.

In Slovenia, abandoned agriculture lands in the karst region are known to go through some successional stages such as grasslands and woody ecosystems (Ferlan et al., 2016; Kaligarič et al., 2006). Each succession stage has a different carbon balance. In fact, while forests are known to act as a sink accumulating carbon in their woody biomass (Ferlan et al., 2016; Pan et al., 2011; Post and Kwon, 2000), grasslands may act as a source of carbon (Ferlan et al., 2011) particularly in periods of drought when the lack of precipitation can decrease photosynthetic carbon uptake (Arnone III et al., 2008; Gilmanov et al., 2007; Meyers, 2001), or as a consequence of other disturbances (e.g. fire events). This led to a poor recognition of the role of grassland ecosystems in the global carbon cycle (Hall et al., 1995; Hall and Scurlock, 1991). However, grasslands play a tremendous role as they stock an important amount of carbon in their soils, estimated at 23% of the global soil carbon (Buringh, 1984). Given this fact, it is important to study the extent of carbon sequestration in grasslands and understand how they contribute in mitigating the effects of climate change.

The Eddy Covariance (EC) method permits to measure, at ecosystem scale, the atmosphere-ecosystem exchange of water, energy and CO_2 fluxes (Papale et al., 2006). The method consists of measurements of the net exchange of gases between the atmosphere and the ecosystem above the canopy where turbulence can be considered more or less constant (Ferlan, 2013). It has been used for the first time in the 1970s (Baldocchi et al., 1988; Desjardins, 1974) and since then has been widely employed in different ecosystem types around the world (Baldocchi, 2008; Ferlan et al., 2011, 2016; Haszpra et al., 2005; Y.-L. Li et al., 2008; Peichl et al., 2012; Ruimy et al., 1995; Saigusa et al., 2002; Yan et al., 2015; Yao et al., 2018). The eddy covariance method provides a reliable direct measurement of different gas compounds together with meteorological variables, at high temporal detail, permitting to ascertain the influence of climate drivers or other disturbances on ecosystem fluxes (Burba and Anderson, 2010).

The eddy covariance measurements represent fluxes in an area around the tower (named footprint), the size and shape of which depend on the set-up of the equipment, the structure and height of the canopy and varies with prevalent wind direction and speed. Usually, the footprint extends over a distance ranging from tens of meters to more than 1km from the tower (Göckede et al., 2008). In the Slovenian karst grassland, footprint analyses showed that the mean distance from the tower is about 195 m (Ferlan, 2013). This spatial limitation raises the necessity to find a way to estimate carbon fluxes outside the

footprint of the eddy covariance tower, since it would be costly and unfeasible to install towers to cover all areas of interest.

NEE is the result of the balance between two components, the respiration of the ecosystem (R_{eco}) and the Gross Primary Productivity (GPP), which represents the amount of carbon fixed through photosynthesis. A possible approach to estimate GPP outside the limits of the footprint of an eddy covariance tower is the use of remotely sensed information. In fact, optical data such as satellite images can be applied to estimate carbon fluxes by establishing relationships between remotely sensed information and fluxes in order to extrapolate GPP outside the boundaries of a tower footprint. Reflectance values obtained from remote platforms in specific wavelengths are generally employed to calculate normalized differences to obtain spectral vegetation indices (VIs).

Light-Use Efficiency models are the most frequently applied to estimate GPP from vegetation indices (VIs) remotely retrieved (Nestola et al., 2016). Besides LUE models, empirical models based on the relationship observed between VIs and GPP are also frequently applied (Gilmanov et al., 2005; Zhengquan Li et al., 2007; Nestola et al., 2016; Rossini et al., 2012). In addition, since photosynthesis (GPP) and respiration (R_{eco}) are generally positively correlated (Baldocchi, 2008; Baldocchi et al., 2015; Ma et al., 2016), it is often possible to infer both NEE and GPP from remote sensing products.

The general objective of this study is to estimate NEE and GPP for a karst grassland in the Podgorski Kras plateau by combining both eddy covariance and satellite data in order to provide a basis for large-scale monitoring of the carbon balance in the Podgorski karst grassland.

In order to reach that objective, this study aims to:
i) Evaluate the ability of different VIs retrieved from remote sensing platforms to represent GPP and NEE trends in a karst grassland,
ii) Compare the performance of different models, integrating VIs in the estimation of GPP and NEE,
iii) Apply obtained results to map NEE and GPP for a grassland area in the Podgorski Kras Plateau.

2. State of the art

2.1. Principle of the eddy covariance method

Airflow consists of numerous eddies. The general principle of eddy covariance measurements can be understood as the covariance between the concentration of interest and vertical wind speed in the eddies (Burba and Anderson, 2010). Put simpler, it consists of measuring how many particles of a component of interest are moving up and down over time and how fast they are (Ferlan, 2013). The horizontal airflow over an investigated area is composed of numerous rotating eddies that can be represented at a single point on the tower by the Figure 1. At a given moment (time 1), eddy 1 moves air parcel c_1 downward with the speed w_1. At the same point, the next moment (time 2), eddy 2 moves air parcel c_2 upward with speed w_2. Given that each air parcel has its own characteristics i.e. gas concentration,

temperature, humidity, etc., if these characteristics and the speed of vertical air movement are measured, the vertical upward or downward fluxes can be known (Burba and Anderson, 2010).

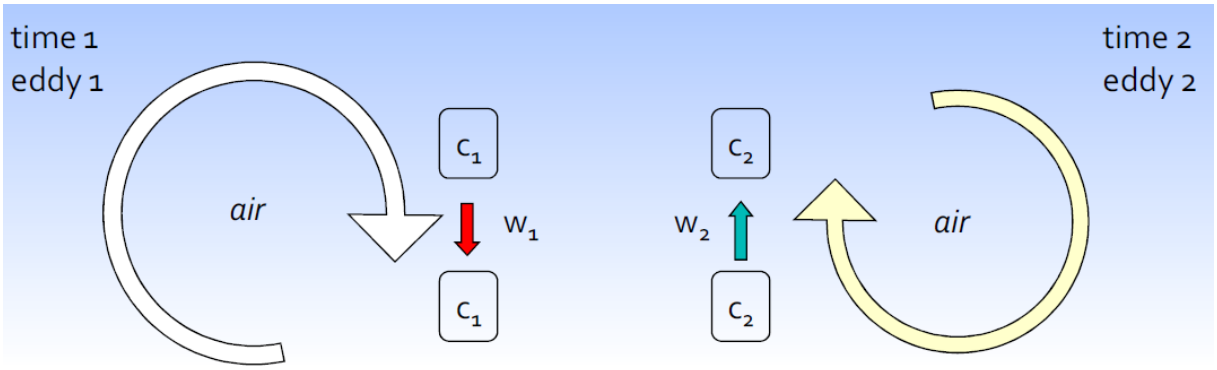

Figure 1: Schematic representation of eddy covariance principles. Source (Burba and Anderson, 2010)

The eddy covariance method has the advantage of performing direct measurements for different types of gas (CO_2, H_2O, CH_4, etc.), with high precision and detail (Burba and Anderson, 2010). However, there are some problems related to the eddy covariance method. The main problem is the occurrence of gaps in the data, which need to be filled by statistical regressions with different methods. Gaps occur due to power breaks (mostly when power system is based on solar panels), damages to instruments, for instance, due to animals or lightning (Aubinet et al., 2012). In addition, equipment malfunctioning such as the anemometers that might not work during heavy precipitation events would make the eddy covariance system glitch during rainy periods (Ferlan, 2013). Another limitation of the method is its restriction to flat areas (Burba and Anderson, 2010).

The Net ecosystem Exchange (NEE) of CO_2 between the atmosphere and the biosphere measured by eddy covariance can be partitioned into the two components of carbon fluxes, Gross Primary Productivity (GPP) and ecosystem respiration (R_{eco}) (Lasslop, Reichstein, Papale, et al., 2010; Reichstein et al., 2005). GPP refers to the total amount of carbon fixed in the process of photosynthesis by plants in an ecosystem; R_{eco} is the amount of carbon lost by autotrophic and heterotrophic respiration. NEE refers to the balance between GPP and carbon losses due to ecosystem respiration (Aubinet et al., 2012; Kirschbaum et al., 2001) as in the equation (1) hereafter.

$$NEE = GPP + R_{eco} \qquad (1)$$

Where NEE is the Net Ecosystem Exchange, GPP is the Gross Primary Productivity and R_{eco} is the Ecosystem Respiration. We adopted in this study the atmospheric sign convention where a flux toward the surface (carbon uptake, i.e. GPP) is negative whereas a flux upward the atmosphere (carbon release, i.e. R_{eco}) is positive (Baldocchi, 2008; Lasslop, Reichstein, Detto, et al., 2010). Consequently, a negative NEE indicates that the ecosystem is acting as a carbon sink while a positive NEE indicates that the ecosystem is acting as a source of carbon.

2.2. Carbon fluxes estimates integrating remote sensing data

With the increasing availability of spatial data thanks to technological progress (Lillesand et al., 2004), their integration into GPP models raised considerably (Mäkelä et al., 2007). LUE models are the most widely used models for integrating carbon fluxes and optical measurements (Lees et al., 2018; Nestola et al., 2016), thanks to the ease of applicability, with the possibility to retrieve indirectly all variables (Bagnara et al., 2018).

LUE models can be expressed in a general form as follows (Yuan et al., 2014):

$$GPP = PAR * fAPAR * LUE_{max} * M \qquad (2)$$

Where PAR is the incident photosynthetically active radiation (MJ m^{-2}); fAPAR is the fraction of absorbed photosynthetically active radiation; LUE_{max} is the potential LUE (g C m^{-2} MJ^{-1} APAR) under ideal environmental conditions; and M is a modifier that depends on environmental conditions, and constrains LUE_{max} to its actual value.

One main limitation of LUE models is related to the LUE_{max} term in the models. It is expressed as a biome-specific constant in most of the models (Goerner et al., 2011; Rossini et al., 2012).

In grasslands, APAR can be assumed to explain most of the variability in GPP (Lobell et al., 2003) and therefore LUE ($LUE_{max}*M$ in equation 1) is generally considered constant (Nestola et al., 2016). However, considering LUE as a constant leads often to errors in the estimate of GPP. In their study, Nestola et al. (2016) obtained better results splitting the analysis in two parts (greening and senescence phases) along the growing season. By doing so, and considering a different LUE for each of the 2 periods, carbon fluxes were more accurately estimated.

Ground cover and leaf area are significant variables that determine absorption of PAR by the canopy. Thanks to the empirical relation that exists between fAPAR and vegetation indices (Running et al., 2004; Yuan et al., 2014), the latter are used in many studies as proxy of carbon fluxes (Nestola et al., 2016; Yan et al., 2015; Y. Zhou et al., 2014). In fact, given the robust relationship between fAPAR and Leaf Area Index (X. Zhou et al., 2002), the fAPAR can be determined based on vegetation indices derived from remote observations of surface spectral reflectance (Myneni and Williams, 1994).

Despite the increasingly available panoply of vegetation indices, their use for estimating fAPAR has been limited to one or two (Y. Zhou et al., 2014). Some of the most widely used indices include NDVI and EVI (Yan et al., 2015; Y. Zhou et al., 2014). In fact, NDVI and fAPAR increase with ground cover and plant leaf area, and their good relationship made it possible to estimate fAPAR from NDVI in many studies (Myneni and Williams, 1994). Nestola *et al.* (2016) confirmed the effectiveness of NDVI as a metrics of green biomass, making it a useful parameter in a simple expression of the LUE model for a grassland ecosystem.

Despite NDVI being a good metrics of green vegetation, it is quite sensitive to background reflectance and tends to saturate at high leaf area. In such conditions, EVI could be employed as an alternative to NDVI because it is less sensitive to these limitations (Rocha and Shaver, 2009).

Other vegetation indices similar to NDVI and EVI could also be explored. For instance, by using the Green instead of the Red band for the calculation of NDVI, the Green NDVI (GNDVI) is more sensitive to chlorophyll content in plants than NDVI (Gitelson et al., 1996). The Soil Adjusted Vegetation index (SAVI) is modified from NDVI by including a soil-adjustment factor (Jovanović et al., 2016).

To overcome the main limitation of LUE models (difficulties in the estimation of the LUE term of the models), some authors attempted to estimate NEE or GPP through linear regression, considering vegetation indices as independent variables (Nestola et al., 2016; Rossini et al., 2012).

In these empirical models, other satellite-derived indices not only related with fAPAR can be explored, for example vegetation indices known to be able to depict surface water content. These indices include the Normalized Difference Senescent Vegetation Index (NDSVI), the Land Surface Water Index (LSWI) and the Modified Normalized Difference Water Index (MNDWI) (Hill, 2013; John et al., 2008; Yan et al., 2015). Water-related vegetation indices can be very good indicators of plant activity in summer when other vegetation indices could be stationary due to some greenness of the plants despite the very low photosynthetic activity. In fact, they are more sensitive to drought than greenness related vegetation indices (Bajgain et al., 2015).

While vegetation indices, and NDVI in particular, proved in many cases to be effective in approximating GPP through the fAPAR component in a LUE model (Myneni and Williams, 1994; Nestola et al., 2016), they are less correlated with ecosystem respiration making R_{eco} usually the most important source of uncertainty in NEE estimation through remote sensing (Yan et al., 2015). Moreover, ecosystem respiration is the sum of heterotrophic (microbes, soil fauna) and autotrophic (plant roots) respiration (Bond-Lamberty et al., 2004; Hanson et al., 2000), which would make its estimation more difficult in some complex ecosystems involving important contribution of heterotrophic respiration. However in some cases it was possible to estimate NEE adopting models integrating remote sensing products (e.g. Nestola et al. 2016).

3. Materials and Methods

3.1. Study area

The present study was conducted in the Podgorski Kras plateau located in the sub-mediterranean region of south-west Slovenia. The area underwent major human influences, due to its position at the transition between the Mediterranean and central Europe. In fact, agricultural practices such as overgrazing in the past centuries led to a pronounced destruction of the vegetation cover, causing severe soil erosion and resulting into a stony and bare landscape. However, thanks to the economic development causing the

near-abandonment of agriculture practices in the area, a succession is taking place and we can observe in the plateau different vegetation types ranging from grasslands to secondary oak forests (Ferlan, 2013).

The bedrock is mainly composed of limestone from Paleocene and Eocene (Knez et al., 2015). The chemical weathering known as karst phenomena led to the formation of Leptosols and Cambisols, which represent insoluble fractions of carbonates. As a result, the soil is superficial, with depths ranging from 0 cm to several decimeters in soil pockets between rocks. The organic matter represents about 12-15% of the topsoil (Ferlan, 2013).

The climate of the area is transient between mediterranean and continental. It is more humid than a typical Mediterranean climate, with less pronounced dry period in summer and colder winter. It is often referred to as sub-mediterranean climate, with a mean annual temperature of 10.5°C, a mean daily temperature of 1.8°C and 19.9°C in January and June respectively, and an average annual precipitation around 1370 mm. Climate statistics represent 30 years average (1971-2000) of four meteorological stations in the sub-mediterranean region (EARS, 2018). Winters are windy (Bora wind), with a periodic snow cover. The growing season ranges from March or April to October (Ferlan, 2013).

This study was limited to a homogenous area of grassland (Figure 2), where only herbaceous species are present with the exception of few shrubs. The most abundant grassland species are *Bromopsis erecta* (Huds.) Fourr., *Carex humilis* Leyss., *Stipa eriocaulis* Borb., *Centaurea rupestris* L., *Potentilla tommasiniana* F.W. Schultz, *Anthyllis vulneraria* L., *Galium corrudifolium* Vill. and *Teucrium montanum* L.

In order to monitor CO_2 and H_2O fluxes between extensive grassland and atmosphere, an eddy covariance tower was installed at the position indicated in Figure 2 (13°55’27.714”E; 45°33’2.858”N) since 2008 (Ferlan et al., 2011), providing measurements of carbon Net Ecosystem Exchange (NEE) and evapotranspiration between the atmosphere and grassland ecosystem.

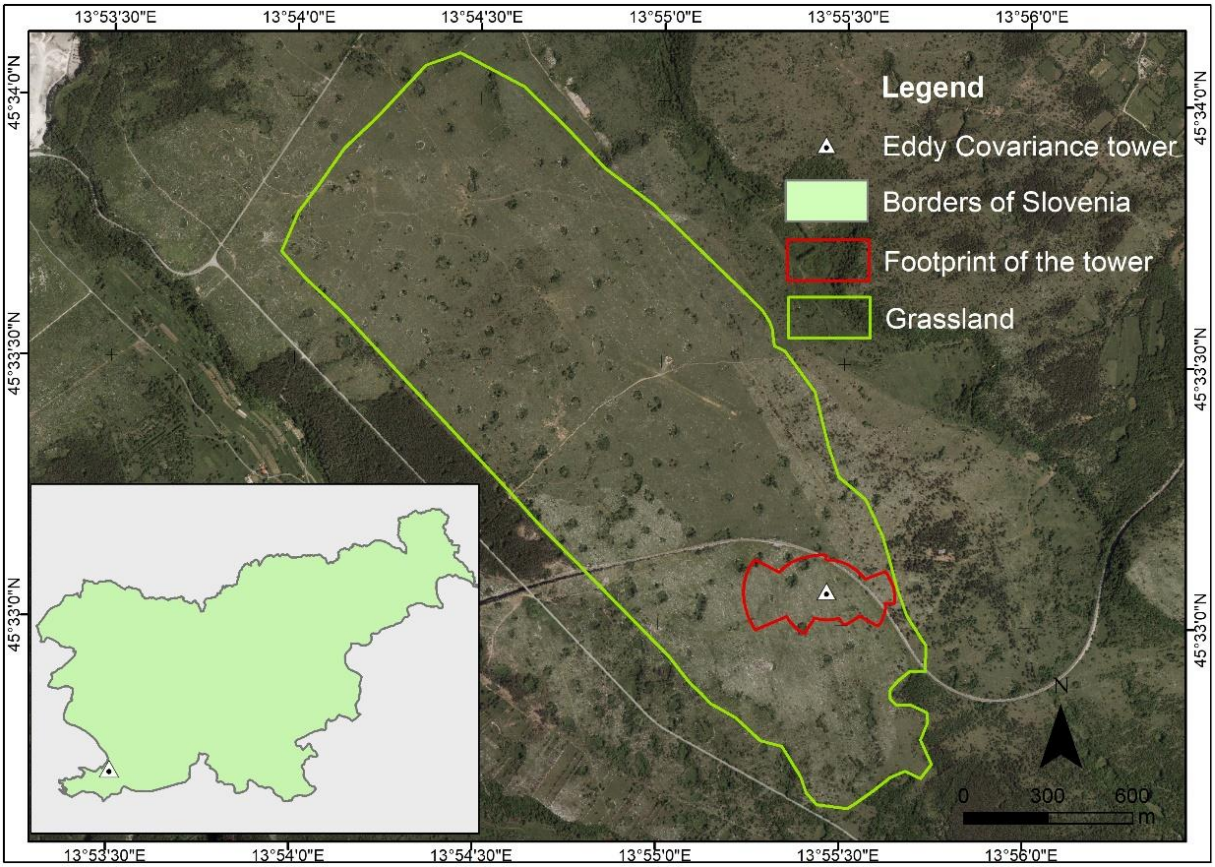

Figure 2: Study area, a karst grassland

3.2. Data acquisition

3.2.1. Eddy Covariance and meteorological data

Apart from an eddy covariance system, a weather station was also installed on the grassland since July 2008. The eddy covariance system consists of an open path infrared gas (CO_2 and H_2O) analyzer (LI-7500, Li-Cor, Lincoln, NE USA) and a sonic anemometer (USA-1, Metek GmbH, Elmshorn, Germany) installed at 2 m height. Flux data were recorded at 20 Hz and then averaged on a half-hourly step. The weather station provides measurements of environmental variables such as soil temperature, soil water content, incident radiation, incident and reflected photosynthetic flux density, net radiation, air temperature, humidity, soil heat flux and precipitation. All measurements of environmental variables were done at 0.1 Hz and then averaged half-hourly (Ferlan et al., 2011).

Air temperature and global radiation data were gapfilled based on data from a meteorological station located in Koper (at a distance of 15 Km from the tower). NEE data were partitioned into GPP and R_{eco} according to Lasslop et al. (2010) using daytime data-based estimates, considering temperature sensitivity of respiration and VPD limitation of GPP.

3.2.2. Spectral vegetation indices

In this study, two sources of data were considered. The 300m resolution NDVI data, consisting of 10 days aggregates of NDVI, provided by the SPOT-Vegetation mission and available for the whole world since 2014 were downloaded from Copernicus global land service portal (CGLSP, 2017). Landsat 8 Operational Land Imager (OLI) images (30m resolution) were downloaded from the portal of the United States Geological Survey (USGS, 2018) for the growing season (March to October) from 2014 to 2017. Landsat 8 images have a temporal resolution of 16 days. However, cloud cover rendered most of them useless (Saranya, 2014; Sun et al., 2017) in our study. Therefore, selected images included all available images with no or insignificant cloud cover in the footprint of the tower. Contrarily to SPOT-Vegetation NDVI data, Landsat images represent single date images. The Table 1 presents the different bands of Landsat 8 and those of SPOT-Vegetation satellite.

Once downloaded, the Landsat images underwent a radiometric calibration to convert radiance values to Top of Atmosphere reflectance, followed by an atmospheric correction through Dark Object Subtraction in order to remove atmospheric components such as scattering and absorption of solar energy in the atmosphere and obtain Top of Canopy reflectance (Chavez, 1996). The image processing was conducted with the ENVI 5.1 software.

Table 1: Spectral range of Landsat and SPOT-Vegetation bands

Name	Landsat range (µm)	SPOT-Vegetation range (µm)
Ultra Blue (coastal/aerosol)	Band 1 (0.435 – 0.451)	–
Blue	Band 2 (0.452 – 0.512)	Band 1 (0.430 – 0.470)
Green	Band 3 (0.533 – 0.590)	–
Red	Band 4 (0.636 – 0.673)	Band 2 (0.610 – 0.680)
Near Infrared (NIR)	Band 5 (0.851 – 0.879)	Band 3 (0.790 – 0.890)
Shortwave Infrared (SWIR) 1	Band 6 (1.566 – 1.651)	Band 4 (1.580 – 1.750)
Shortwave Infrared (SWIR) 2	Band 7 (2.107 – 2.294)	–
Panchromatic	Band 8 (0.503 – 0.676)	–
Cirrus	Band 9 (1.363 – 1.384)	–
Thermal Infrared (TIRS) 1	Band 10 (10.60 – 11.19	–
Thermal Infrared (TIRS) 2	Band 11 (11.50 – 12.51)	–

The corrected images were used to compute a variety of vegetation indices (Table 2), namely the Normalized Difference Vegetation Index (NDVI), the Green Normalized Difference Vegetation Index (GNDVI), the Enhanced Vegetation Index (EVI), the Land Surface Water Index (LSWI), the Modified Normalized Difference Water Index (MNDWI), the Soil Adjusted Vegetation Index (SAVI), and the Normalized Difference Senescent Vegetation Index (NDSVI).

For NDVI data from the SPOT-Vegetation mission (NDVIs) (directly downloaded from the Copernicus global land service portal) and all vegetation indices computed from Landsat images (Table 2), an

average value was computed for the pixels in the footprint (Figure 2) using the Raster package in R software.

Table 2: Vegetation indices adopted for this study

Satellite	Index	Formula	Reference
SPOT	NDVIs	$NDVIs = (b_3 – b_2) / (b_2 + b_3)$	Rouse *et al.* (1974)
L8	NDVI	$NDVI = (b_5 – b_4) / (b_5 + b_4)$	Rouse *et al.* (1974)
L8	GNDVI	$GNDVI = (b_5 - b_3) / (b_5 + b_3)$	Gitelson et al. (1996)
L8	EVI	$EVI = (2.5 * (b_5 – b_4)) / (b_5 + 6*b_4 – 7.5*b_2 + 1)$	Huete *et al.* (2002)
L8	NDSVI	$NDSVI = (b_6 – b_4) / (b_6 + b_4)$	John et al. (2008)
L8	SAVI	$SAVI = ((1 + L)(b_5 – b_4)) / (b_5 + b_4 + L)$	Huete (1988)
L8	LSWI	$LSWI = (b_5 - b_6) / (b_5 + b_6)$	Xiao et al. (2005)
L8	MNDWI	$MNDWI = (b_3 – b_6) / (b_3 + b_6)$	Xu (2006)

L is a constant dependent on the vegetation cover and takes values from 0 (for very green vegetation) to 1 (areas with no green vegetation), assumed 0.5 here.

Despite the availability of flux data since 2008, only a timeframe of four years was considered in order to match the timeframe of the remote sensing information used in this study.

3.3. Data analysis

In this study, we considered two types of aggregation of flux data. The first type of aggregation consisted of midday average of half-hourly fluxes between 11 am and 4 pm as in Nestola et al. (2016). The second type of aggregation consisted of daily average of half-hourly fluxes. For further analysis, midday or daily flux data were subsequently grouped at different time steps. For NDVIs data, midday or daily flux data were subsequently averaged over 10 days period to match temporal aggregation provided by SPOT-Vegetation. For VIs derived from Landsat 8 images, midday or daily flux data were subsequently averaged over 5 days (4 days prior to the date of each image) since a preliminary test showed a better correlation if aggregated fluxes were considered instead of fluxes of the overpass day only.

Three types of model after Rossini et al. (2012) were tested in this study:

i) Model 1 assuming a direct linear relationship between GPP or NEE and a vegetation index

$$NEE \text{ or } GPP = a*VI + b \qquad (3)$$

ii) Model 2 assuming a direct linear relationship between GPP and the product of a vegetation index and PAR

$$GPP = a*(VI*PAR) + b \qquad (4)$$

iii) Model 3, a LUE model assuming a constant LUE and fAPAR estimated as a linear function of a vegetation index

$$GPP = (a*VI+b)*PAR \qquad (5)$$

All models were tested for the entire growing season (single) or splitting the growing season in two phases (green and dry). The separation of the growing season was based on preliminary tests during which we plotted GPP or NEE as a function of VIs and tried a separation based on months. The months of June, July and August allowed a visual identification of a different group. However, the separation

was not perfect and different values of midday aggregates of Tair and VPD (averaged over 10 days for SPOT-Vegetation NDVIs and 5 days for Landsat VIs) were tried instead of months. VPD proved to be the best for separating the growing season into 2 phases, with a threshold of 1500 Pa. We defined the greening phase as the period of the growing season with midday average VPD less than or equal to 1500 Pa, and the dry phase as the period of the growing season with midday average VPD greater than 1500 Pa.

In order to compare the performance of the models obtained from the different regressions, three accuracy metrics were computed, namely the coefficient of determination (R^2), the Root Mean Square Error (RMSE) and the Akaike Information Criterion (AIC). The best models are the ones with a high value of R^2 and a low value of RMSE and AIC.

All analyses were done using the R software, version 3.4.4.

The best models selected were used to create illustrative GPP and NEE maps of the study area for two dates. The choice of the dates only aimed at having one in the greening phase and another one in the dry phase. Image algebra was performed on a vegetation index layer based on the expression of each model. When required in the expression of the model, PAR was used with the proper aggregation, i.e. midday or daily aggregate, 10 or 5 days average, depending on which aggregate of flux is being estimated and which source of vegetation index is being considered (SPOT-Vegetation or Landsat 8). The maps were created using the ArcGIS 10.4.1 software. The resulting GPP and NEE represent average fluxes of 5 or 10 days if estimated from Landsat derived VIs or NDVIs respectively.

4. Results

4.1. Carbon fluxes and environmental variables

The Figure 3 below presents, for the period 2014-2017, fluxes (NEE, GPP, R_{eco}) and some main environmental variables including vapor pressure deficit (VPD), air temperature (Tair), global radiation (Rg) and precipitation (P). Large gaps are noticeable for flux data and VPD, whereas Tair and Rg show no gaps because they were gap-filled from another meteorological station.

GPP shows some seasonality and has two peaks during the growing season, a high peak around end of May or beginning of June and a low peak in October. In between the two peaks, there is a period of low carbon uptake translating into low GPP values in July and August. Similar trends were visible in NEE and Reco. In fact, a strong correlation was observed between NEE and GPP, both for midday and daily averages (Figure 5).

The maximum values of VPD and Tair match the low GPP period. Global radiation however reaches its yearly peak earlier than VPD and Tair, somewhere between May and June.

Precipitation data shows no real pattern of seasonality, as the distribution over the year seems quite random. However, there is generally less precipitation in July and August than in any other months, in some years.

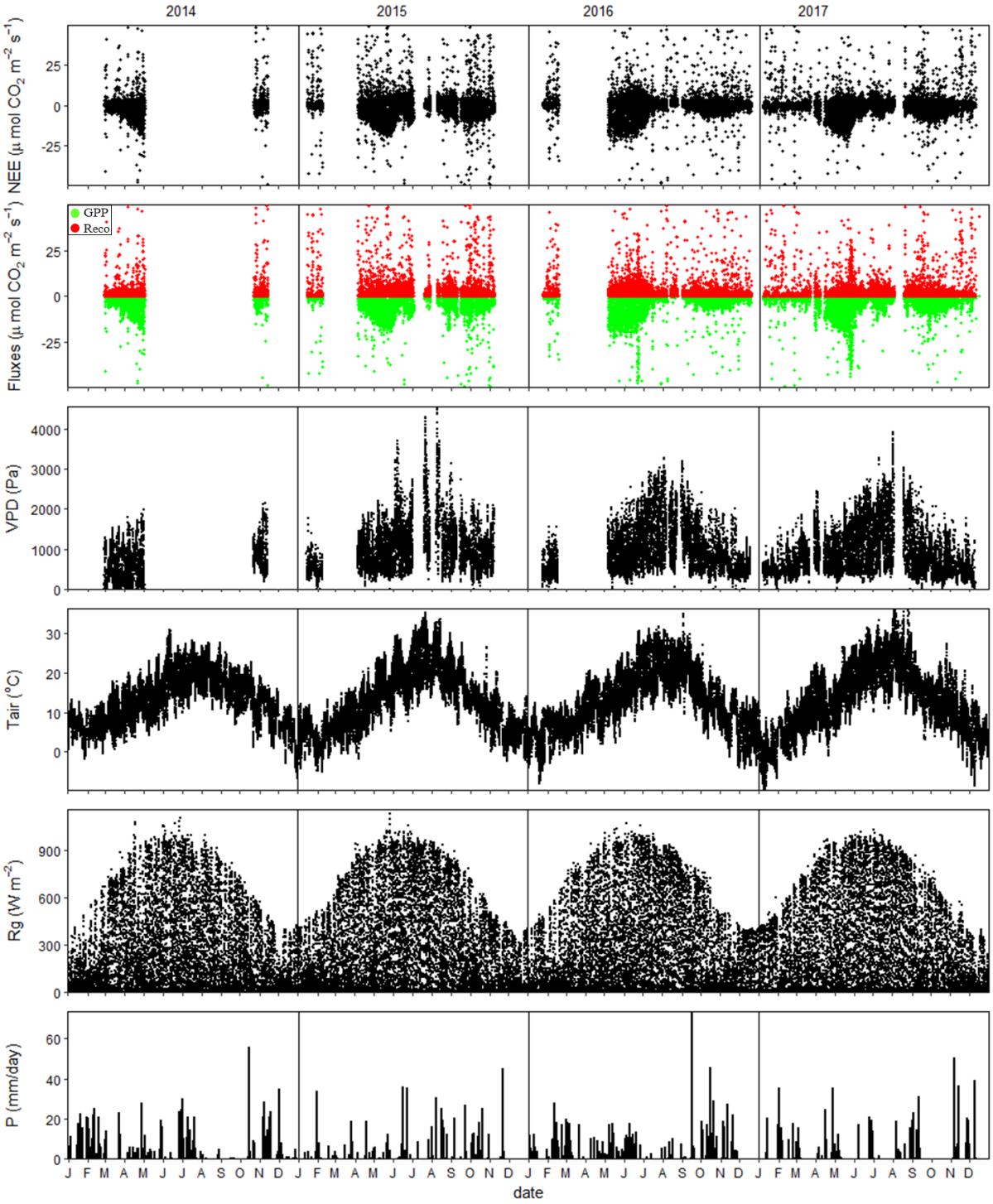

Figure 3: Thirty minutes averages of carbon fluxes, VPD, Tair, Rg and total daily precipitation recorded between 2014 and 2017 in the karst grassland.

4.2. Vegetation indices

The Figure 4 represents all the spectral vegetation indices used in this study. All the vegetation indices that represent vegetation greenness (NDVI, EVI, SAVI and GNDVI) have quite similar trends. In addition, NDVI from the two different sources (Landsat and SPOT-Vegetation) match quite well, with the difference that NDVIs has slightly higher values than NDVI. All these vegetation indices increase from the beginning of the growing season, to reach a peak around end of May or beginning of June. They start decreasing slowly for about 3 months. Around September, there is again a slight increase in the vegetation index. This last increase is better seen with NDVIs.

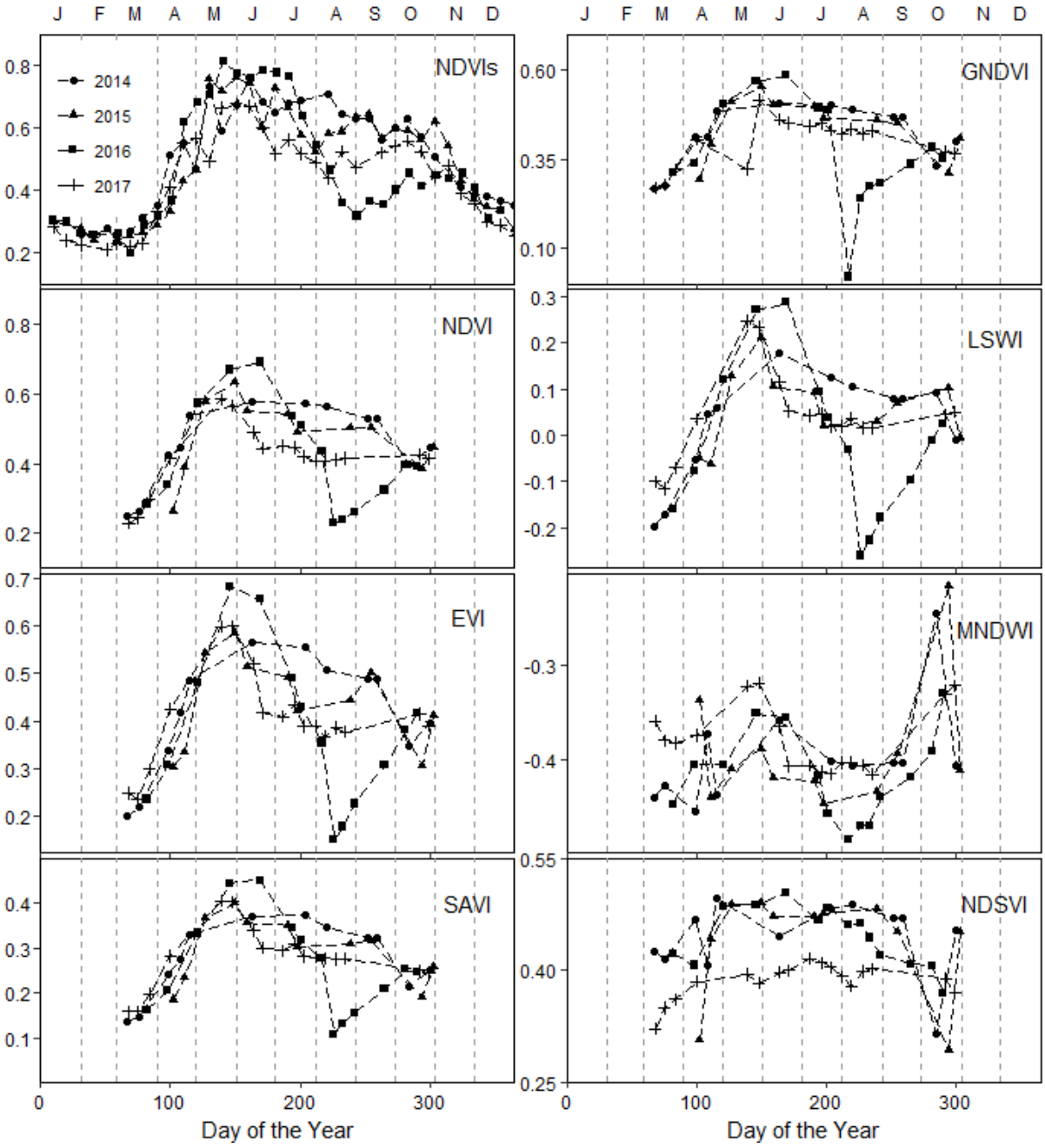

Figure 4: Temporal profile of vegetation indices calculated in this study (see Table 2). Different symbols represent different years.

The year 2016 shows an unusual trend, with a very low value recorded for some vegetation indices in August, due to a fire that occurred at that period. This unexpected disturbance was visible in GNDVI, NDVI, EVI, SAVI, LSWI and MNDWI, but less visible in NDVIs and NDSVI.

LSWI is a water-related vegetation index, but it has a trend that is similar to the greenness-related vegetation indices. This can be explained by the fact that vegetation greenness reflects the water content in plant leaves, which is detected through LSWI. MNDWI on the contrary has an overall different trend since it is really meant to detect water bodies (Xu, 2006), but it also shows a decrease during the months of June, July and August. NDSVI, which is also a water-related vegetation index, does not decrease during June, July and August as MNDWI.

These observations about the vegetation indices along with the trend of fluxes and environmental variables suggest that the growing season can be subdivided in two phases, a greening phase (March to May/June and September to October) and a dry phase (June to August) when the higher Tair and VPD, together with a decrease in precipitation lead to a decrease in GPP. However, these two phases could not be clearly defined by months, since climate is quite variable from one year to another. Our separation, based on VPD instead of months, proved to better split the two phases of the growing season with the threshold of 1500 Pa.

4.3. Correlation charts of fluxes and vegetation indices

The Figure 5 shows a correlation matrix of fluxes (NEE and GPP) with all vegetation indices. The good relationship between most vegetation indices, as mentioned previously, is confirmed by the high correlation coefficients observed. MNDWI and NDSVI are poorly correlated with the other vegetation indices.

On the correlation charts, only separate fit lines are showed in order not to make the graphs overloaded (left bottom of the matrix). However, correlation coefficients were computed also for the single fit (values in black in the matrix). Low correlation coefficients were obtained for the single fit whereas the consideration of the two phases of the growing season gave higher correlation coefficients.

All the greenness-related VIs (NDVIs, NDVI, EVI, SAVI and GNDVI) and LSWI gave higher correlation coefficients in the greening phase compared to the dry phase for GPP (both midday and daily aggregates) and midday NEE. For daily NEE aggregates, those VIs except GNDVI gave a better correlation coefficient during the dry phase instead. MNDWI gave high correlation coefficients during the dry phase for GPP and NEE, both for midday and daily aggregates. NDSVI gave better correlation coefficients during the greening phase than the dry phase for GPP and NEE with both aggregates, but generally lower than correlation coefficients observed with other VIs.

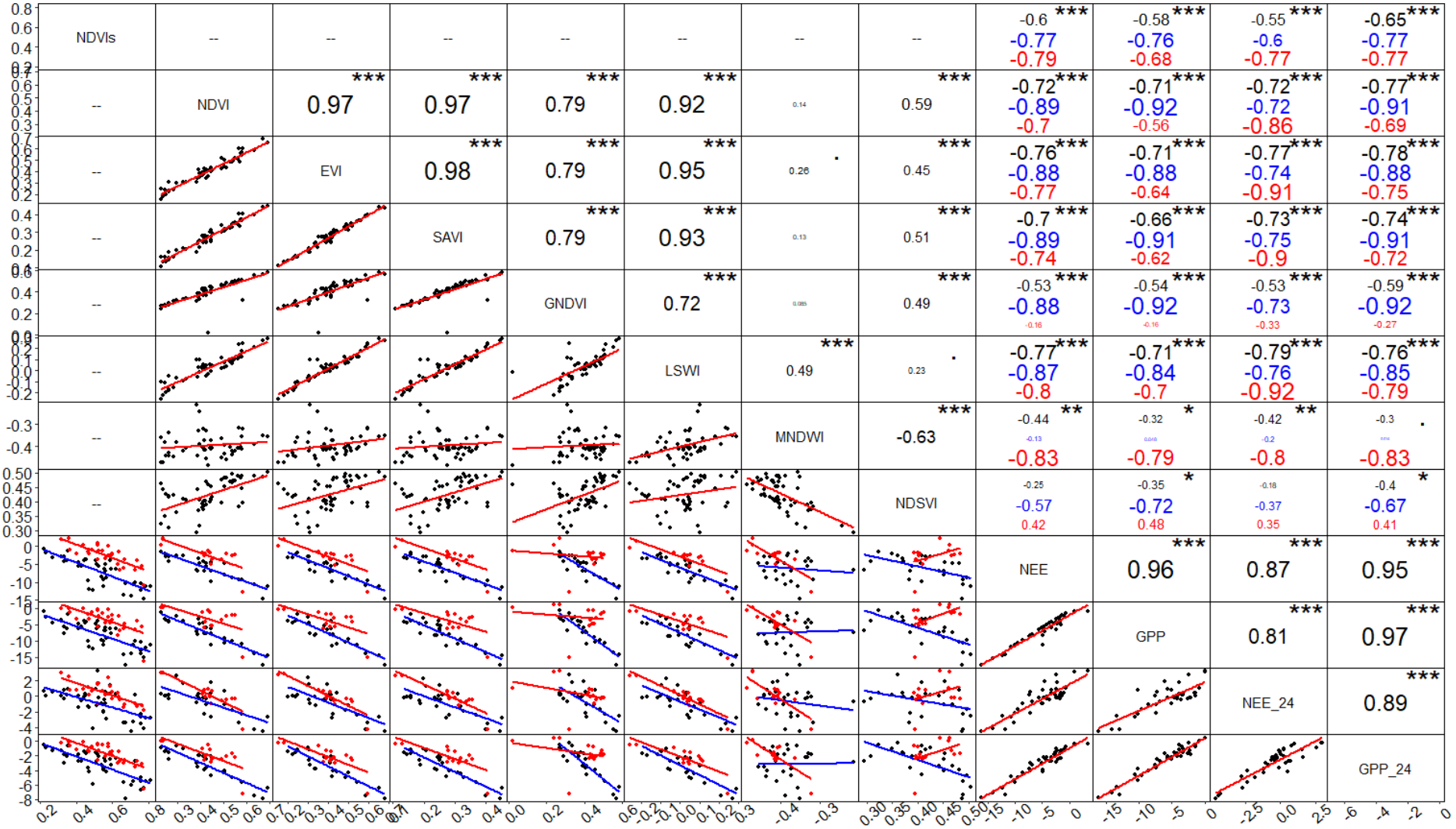

Figure 5: Correlation charts between fluxes and vegetation indices. Values in black, blue and red represent Pearson correlation coefficients for a single fit, the greening phase (VPD < 1500 Pa) and the dry phase (VPD > 1500 Pa) respectively. The remark "_24" is used to distinguish daily average fluxes from midday average fluxes. *, **, *** indicates correlations significant at 95%, 99% and 99.9%

Midday average fluxes generally show a better correlation with VIs than daily averages during the greening phase, while the opposite was observed during the dry phase. This observation was the same both for GPP and NEE. The best correlation coefficients observed for midday averages during the greening phase could be due to less fluctuation in the midday average fluxes due to the reduced time scale considered and the fact that most carbon uptake occur around midday during that phase of the growing season. During the dry phase however, there is less carbon uptake during the day, and midday averages may fluctuate more depending on particular environmental conditions of every single day (higher temperatures of some days may lead to more respiration). Daily averages would hide those fluctuations, explaining why we obtained better correlations with VIs than midday averages during the dry phase.

4.4. Comparison of the different models

The Table 3 shows values of accuracy metrics for the three types of model considered in this study, for midday average fluxes. Similarly, Table 4 shows accuracy metrics considering daily average fluxes. The values of these tables directly reflect trends and correlation coefficients previously presented in Figure 5. No exceptions were found in our study, as high values of R^2 corresponded always to low values of RMSE and AIC. The three metrics are all however useful, since slight differences can be noticed in the RMSE and AIC when R^2 is the same, and this helped in the choice of the best model.

The VIs performed differently from one model to another, according to the phase of the growing season being considered and the flux aggregate being estimated.

What was mentioned in the previous section, about a poor correlation between fluxes and vegetation indices with a single fit, can be confirmed by generally low values of R^2 or higher values of RMSE and AIC. The best model with a single fit considering Landsat VIs was always obtained with LSWI for NEE and EVI for GPP in a direct correlation (model 1), be it with midday average or daily average fluxes. NDVIs however gave lower R^2 values in all models and for both aggregations of flux data (midday and daily) when a single fit for the whole season was considered, and the highest R^2 observed was 0.43.

Overall, separate fits gave higher R^2 and lower RMSE and AIC in all models compared to a single fit. In fact, the highest R^2 obtained in a single fit was 0.59 for midday fluxes and 0.62 for daily fluxes, but it was possible to obtain 0.85 and 0.91 during the greening phase for midday and daily aggregates respectively, 0.69 and 0.86 during the dry phase for midday and daily aggregates respectively.

For the greening phase, NDVI was the best predictor of midday aggregates of GPP and NEE with all three model types. For daily aggregates, NDVI was the best vegetation index only in models 2 and 3 whereas in model 1, LSWI and GNDVI were the best vegetation indices for NEE and GPP respectively.

For the dry phase, MNDWI was the best predictor of midday aggregates of GPP and NEE with all three model types. For daily aggregates, MNDWI was the best VI except in model 2 and model 1 with NEE, where LSWI gave the highest R^2.

Midday fluxes gave higher R^2 than daily fluxes during the greening phase for the model type 1 (direct correlation). However, during the dry phase (all model types) and also the greening phase with models including PAR (2 and 3), daily fluxes gave higher R^2 than midday fluxes.

Table 3: GPP~VIs and NEE~VIs regression accuracy metrics (R^2, RMSE, AIC) obtained using only midday fluxes. For Landsat VIs, the best regression results are highlighted for each type of model and for single, green and dry. For SPOT, the best regression models are highlighted for single, green and dry, all model types together.

			R^2			RMSE(µmol $m^{-2}s^{-1}$)			AIC		
Model	Flux	VIs	single	green	dry	single	green	dry	single	green	dry
1	NEE	**NDVIs**	0.36	**0.59**	**0.62**	3.34	**2.51**	**1.72**	172.83	**81.40**	**34.40**
		NDVI	0.52	**0.80**	0.49	2.87	**1.68**	2.67	88.46	**30.96**	31.54
		EVI	0.58	0.78	0.59	2.70	1.75	2.40	83.60	33.05	28.50
		SAVI	0.48	0.79	0.55	2.99	1.73	2.51	91.71	32.52	29.76
		GNDVI	0.29	0.78	0.03	3.52	1.76	3.68	104.77	33.32	40.49
		LSWI	**0.59**	0.75	0.64	**2.68**	1.88	2.23	**82.96**	36.73	26.52
		MNDWI	0.19	0.02	**0.69**	3.74	3.72	**2.09**	109.60	72.31	**24.68**
		NDSVI	0.06	0.33	0.18	4.04	3.07	3.38	115.73	62.35	38.14
	GPP	NDVIs	0.33	0.58	**0.46**	3.53	2.53	**2.47**	180.56	82.10	**54.57**
		NDVI	0.50	**0.85**	0.32	2.81	**1.42**	2.83	84.48	**21.65**	33.17
		EVI	**0.51**	0.77	0.41	**2.78**	1.74	2.64	**83.62**	31.83	31.18
		SAVI	0.44	0.82	0.38	2.97	1.54	2.71	88.81	25.64	31.88
		GNDVI	0.30	0.85	0.02	3.32	1.43	3.39	97.69	22.04	38.19
		LSWI	0.50	0.71	0.48	2.80	1.99	2.47	84.29	38.33	29.29
		MNDWI	0.10	0.00	**0.63**	3.76	3.67	**2.10**	107.24	68.96	**24.77**
		NDSVI	0.12	0.52	0.23	3.71	2.54	3.01	106.23	50.53	34.81
2	GPP	**NDVIs**	0.10	**0.73**	0.37	4.10	**2.03**	2.67	201.57	**63.61**	58.99
		NDVI	0.19	**0.81**	0.19	3.56	**1.61**	3.10	103.07	**27.92**	35.66
		EVI	0.22	0.75	0.26	3.50	1.82	2.95	101.64	33.96	34.32
		SAVI	0.18	0.77	0.24	3.60	1.76	2.99	103.83	32.30	34.67
		GNDVI	0.10	0.73	0.01	3.75	1.92	3.41	107.11	36.55	38.39
		LSWI	**0.48**	0.74	0.47	**2.85**	1.89	2.51	**85.64**	35.71	29.76
		MNDWI	0.03	0.22	**0.61**	3.90	3.25	**2.13**	110.15	62.90	**25.21**
		NDSVI	0.01	0.55	0.13	3.94	2.45	3.20	110.92	48.83	36.53
3	GPP	NDVIs	0.11	0.73	0.45	4.45	2.07	2.49	212.88	64.97	55.10
		NDVI	0.26	**0.84**	0.25	3.75	**1.67**	2.98	107.03	**29.72**	34.58
		EVI	0.26	0.76	0.33	3.72	1.92	2.84	106.41	36.71	33.24
		SAVI	0.18	0.77	0.31	3.92	1.90	2.87	110.48	36.03	33.52
		GNDVI	0.11	0.80	0.01	4.10	1.81	3.46	114.01	33.80	38.73
		LSWI	0.27	0.74	0.40	3.68	1.99	2.67	105.69	38.32	31.45
		MNDWI	0.08	0.26	**0.53**	3.90	3.15	**2.38**	110.08	61.45	**28.26**
		NDSVI	0.03	0.67	0.18	4.24	2.13	3.13	116.69	41.80	35.92

Table 4: GPP~VIs and NEE~VIs regression accuracy metrics (R^2, RMSE, AIC) obtained using daily fluxes. For Landsat VIs, the best regression results are highlighted for each type of model and for single, green and dry. For SPOT, the best regression models are highlighted for single, green and dry, all model types together.

			R^2			RMSE (µmol $m^{-2}s^{-1}$)			AIC		
Model	Flux	VIs	single	green	dry	single	green	dry	single	green	dry
1	NEE	NDVIs	0.30	0.36	0.59	1.45	1.42	0.80	55.86	33.36	-8.48
		NDVI	0.52	0.52	0.74	1.23	1.21	0.85	20.70	13.92	-0.61
		EVI	0.59	0.55	0.82	1.13	1.17	0.71	13.80	12.31	-5.69
		SAVI	0.54	0.57	0.81	1.20	1.15	0.74	18.98	11.19	-4.61
		GNDVI	0.28	0.53	0.11	1.49	1.20	1.58	36.85	13.46	16.79
		LSWI	**0.62**	**0.58**	**0.86**	**1.08**	**1.13**	0.63	**10.52**	**10.19**	**-8.72**
		MNDWI	0.18	0.04	0.64	1.60	1.71	1.00	42.41	31.89	4.02
		NDSVI	0.03	0.14	0.13	1.73	1.62	1.56	49.18	29.07	16.48
	GPP	**NDVIs**	**0.43**	0.60	0.59	**1.41**	1.18	0.90	**51.77**	17.58	-1.92
		NDVI	0.59	0.82	0.47	1.09	0.71	1.07	11.18	-12.88	5.79
		EVI	**0.62**	0.78	0.57	**1.06**	0.80	0.96	**9.02**	-7.37	2.98
		SAVI	0.54	0.83	0.52	1.16	0.71	1.01	15.93	-13.46	4.33
		GNDVI	0.35	**0.84**	0.07	1.39	**0.68**	1.41	30.31	**-15.27**	13.69
		LSWI	0.58	0.73	0.62	1.11	0.88	0.90	12.36	-2.34	1.08
		MNDWI	0.09	0.00	**0.69**	1.64	1.70	**0.82**	43.39	30.47	**-1.55**
		NDSVI	0.16	0.46	0.17	1.57	1.25	1.34	40.27	15.28	12.15
2	GPP	NDVIs	0.19	0.78	0.52	1.67	0.87	0.98	75.59	-7.60	2.61
		NDVI	0.30	**0.85**	0.32	1.43	**0.66**	1.21	32.78	**-16.99**	9.37
		EVI	0.34	0.81	0.40	1.39	0.74	1.13	30.53	-10.95	7.52
		SAVI	0.28	0.82	0.37	1.46	0.71	1.16	34.06	-12.92	8.14
		GNDVI	0.17	0.78	0.05	1.56	0.79	1.43	39.57	-7.94	14.00
		LSWI	**0.57**	0.76	**0.61**	**1.13**	0.83	**0.92**	**13.47**	-5.47	**1.53**
		MNDWI	0.01	0.25	0.55	1.71	1.47	0.98	47.02	23.16	3.42
		NDSVI	0.05	0.59	0.06	1.67	1.08	1.42	45.02	7.98	13.89
3	GPP	**NDVIs**	0.17	**0.80**	**0.60**	1.74	**0.83**	**0.89**	81.90	**-11.55**	**-2.36**
		NDVI	0.36	**0.91**	0.42	1.52	**0.57**	1.12	37.41	**-24.15**	7.28
		EVI	0.38	0.86	0.49	1.50	0.67	1.06	36.36	-15.84	5.52
		SAVI	0.28	0.87	0.47	1.61	0.66	1.08	41.89	-17.14	6.05
		GNDVI	0.18	0.89	0.06	1.71	0.61	1.42	46.84	-20.45	13.87
		LSWI	0.36	0.86	0.55	1.51	0.68	0.98	36.94	-15.28	3.52
		MNDWI	0.17	0.50	**0.60**	1.59	1.24	**0.93**	41.14	14.66	**2.09**
		NDSVI	0.09	0.77	0.16	1.74	0.82	1.35	48.11	-5.65	12.36

Based on these accuracy metrics, the best regression models are presented in Table 5, according to the two aggregates (midday and daily), sources of vegetation indices (Landsat and SPOT-Vegetation) and fluxes (GPP and NEE) for the two phases of the growing season. Direct correlation (model type 1) was found to be the best option for midday average fluxes, except for the estimation of GPP with NDVIs during the greening phase, where the model type 2 was the best. For daily averages however, the model type 1 performed better with NEE whereas model types 2 and 3 were the best for GPP.

During the greening phase, the best models obtained for GPP gave higher coefficients of determination (R^2) compared to those obtained with NEE. The opposite was observed for the dry phase.

Table 5: Best models selection based on accuracy metrics

Aggregate	VI source	Flux	Greening phase	Dry phase
Midday	Landsat	GPP	-26.34*NDVI+4.17, $R^2=0.85$	-64.9*MNDWI-30.7, $R^2=0.63$
	SPOT		-0.03*(NDVIs*PAR)-0.71, $R^2=0.73$	-19.17*NDVIs+7.17, $R^2=0.46$
	Landsat	NEE	-26.03*NDVI+4.76, $R^2=0.80$	-73.81*MNDWI-33.52, $R^2=0.69$
	SPOT		-19.35*NDVIs+3.13, $R^2=0.59$	-18.49*NDVIs+7.75, $R^2=0.62$
Daily	Landsat	GPP	(-0.044*NDVI+0.004)*PAR, $R^2=0.91$	-29.05*MNDWI-13.93, $R^2=0.69$
	SPOT		(-0.033*NDVIs)*PAR, $R^2=0.80$	(-0.028*NDVIs+0.01)*PAR, $R^2=0.60$
	Landsat	NEE	-10.72*LSWI-0.57, $R^2=0.58$	-12.34*LSWI+0.3, $R^2=0.86$
	SPOT		-6.81*NDVIs+2.61, $R^2=0.36$	-7.97*NDVIs+4.88, $R^2=0.59$

4.5. Flux maps using the best models

The Figure 6 shows a map of fluxes for the study area, computed based on the equations of Table 5. The fluxes represent estimated average NEE and GPP for the periods 15/05/2017 to 19/05/2017 (for Landsat) and 11/05/2017 to 20/05/2017 (for SPOT). Similarly, the Figure 7 shows estimated average of NEE and GPP for the periods 02/07/2017 to 06/07/2017 (for Landsat) and 01/07/2017 to 10/07/2017 (for SPOT). The dates were chosen to have an illustration for both greening and dry phases.

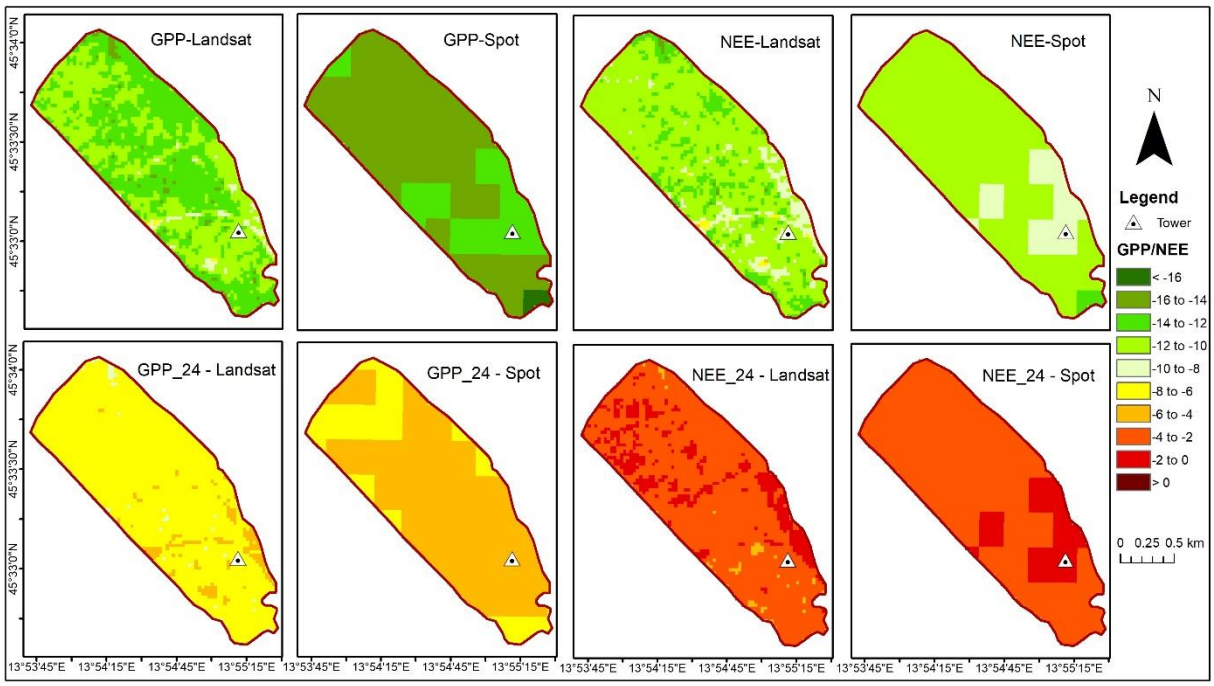

Figure 6: Maps of average midday and daily GPP and NEE estimates for the periods 15/05/2017 to 19/05/2017 (for Landsat) and 11/05/2017 to 20/05/2017 (for SPOT), using the best models obtained for the **greening phase**. The remark "_24" is used to distinguish daily from midday average fluxes.

During the greening phase (Figure 6), GPP or NEE estimated from the two different sources of vegetation indices have similar spatial distributions. The estimates from NDVIs can be considered a generalization of that obtained from Landsat derived VIs. In the case of midday average fluxes, NEE and GPP seem to have the same distribution with differences only in their values. This is a consequence of the very good linear relationship that was found between midday GPP and NEE in our study. Daily

fluxes however show more difference between NEE and GPP, as the correlation observed was not as good as that of midday fluxes.

During the dry phase (Figure 7), the spatial distribution of fluxes is quite different between flux estimates from the two sources of VI (Landsat and SPOT-Vegetation), with the exception of estimates of daily aggregates of NEE, where the estimate from NDVIs appears like a generalization of the estimate from LSWI.

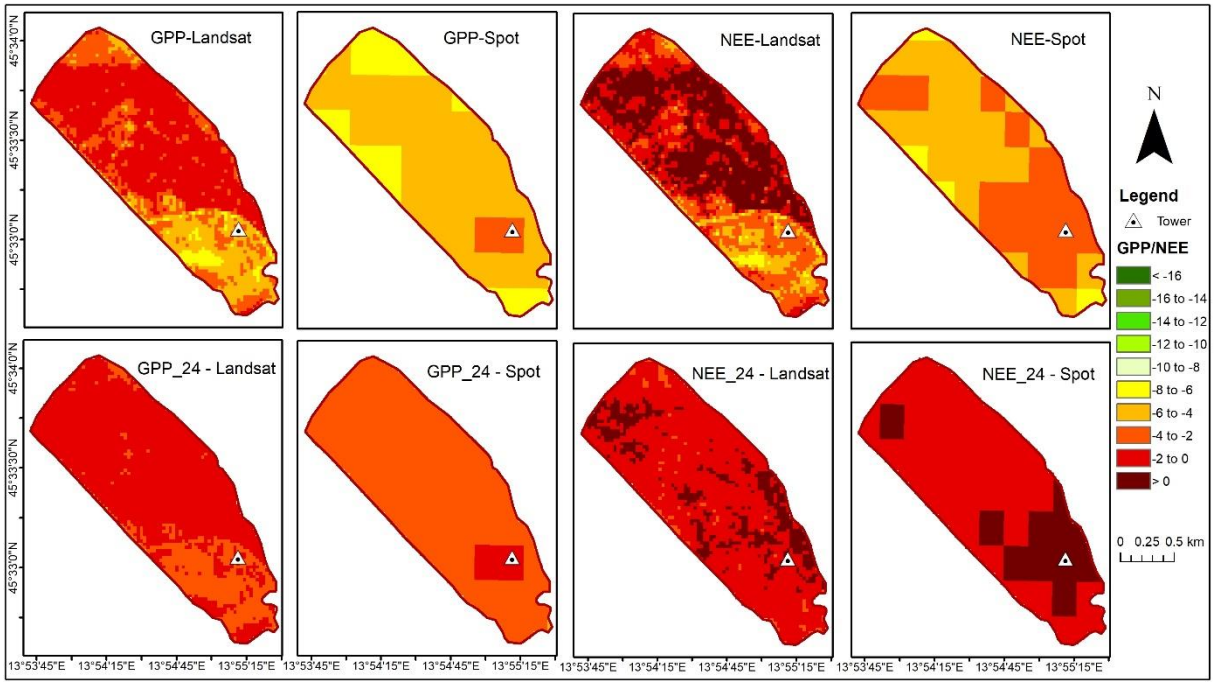

Figure 7: Maps of average midday and daily GPP and NEE estimates for the periods 02/07/2017 to 06/07/2017 (for Landsat) and 01/07/2017 to 10/07/2017 (for SPOT), using the best models obtained for the **dry phase**. The remark "_24" is used to distinguish daily from midday average fluxes.

A difference can be noticed between the greening and the dry phases. GPP estimates are very low during the dry phase, and the carbon balance (NEE estimates) became positive in some parts of the study area.

5. Discussion

Several climatic factors, including temperature, precipitation, solar radiation and water deficit interact to influence the variability observed in carbon fluxes (Griffis et al., 2000), making it difficult to separate their individual effects clearly (Hui et al., 2003). In our study, the low carbon uptake observed during a period of the year (June to August) with high VPD and Tair, and relatively lower precipitation confirmed that climate is a key driver of carbon fluxes. The impact of climatic drivers could be stronger in this karst grassland, characterized by shallow soils. In fact, in ecosystems facing drought periods (due to low precipitation rates and shallow soils), GPP and consequently NEE are primarily controlled by climatic factors such as precipitation (Ferlan et al., 2011). In addition, the fact that grasses use water intensively (Rodriguez-Iturbe et al., 2001) makes precipitation an important variable that affects the variability in carbon fluxes.

The separation of the growing season into two phases as in Nestola et al. (2016) proved to be useful for a better correlation between fluxes and vegetation indices. In our study, the threshold of 1500 Pa for VPD showed to be a threshold across years in spite of differences observed in precipitation.

The good relationship between GPP and NEE (Baldocchi, 2008; Baldocchi et al., 2015; Ma et al., 2016) was confirmed in our study, allowing to infer both NEE and GPP from vegetation indices.

Overall, NDVI was the best predictor for the estimation of NEE and GPP during the greening phase of the growing season, reinforcing the conclusion of previous studies that NDVI is an index of choice for depicting photosynthetic activity (Gamon et al., 1995; Myneni et al., 1995; Nestola et al., 2016) which translates into CO_2 assimilation (GPP component of carbon fluxes). On the other hand, LSWI and MNDWI proved to be ideal for estimating fluxes during the dry period, confirming the fact that water-related vegetation indices are the best indicators of photosynthetic activity during the dry season, as they are more sensitive to water stress than the other vegetation indices (Bajgain et al., 2015). NDSVI, which is also a water-related vegetation index, did not give good results for the dry phase as for LSWI and MNDWI. Other studies reported the low performance of NDSVI in depicting non-photosynthetic vegetation in a semi-arid grassland and a cropland (Zhaoqin Li and Guo, 2018; Sonmez and Slater, 2016), which relates to the low performance observed in our study.

Strong direct correlations were observed between fluxes and vegetation indices (model type 1) as in Rossini et al. (2012). This confirms that APAR (which is highly dependent on the vegetation greenness) explains most of the variability of GPP in an ecosystem characterized by a seasonality in greening and senescence such as grasslands and croplands (Gamon, 2015; Gitelson et al., 2006; Lobell et al., 2003). However, the fact that GNDVI did not perform well generally suggests that chlorophyll content is not the only factor that comes into play in this particular karst grassland, which seemed to have an important water stress influence during the dry phase.

Despite the fire event that occurred in August 2016, which was easy to depict in the VIs profiles, we did not notice any outliers corresponding to that period in our regressions. This might be explained by the occurrence of the fire event towards the end of the dry phase, and the grasses recovered during the second part of the greening phase in September. Indeed, grasslands are known to recover quickly following a fire event (Keeley and Keeley, 1984).

An interesting point about this study is that reasonable results were obtained also for daily fluxes. We consider daily average flux estimates more useful than midday average flux estimates in terms of monitoring the total productivity of an ecosystem. Even though a daily (24 hours) average flux was considered instead of the sum due to missing data, we considered that the average without the missing data represents a good proxy of the total daily flux.

The two sources of vegetation indices (Landsat and SPOT) could not really be compared, given that Landsat images were single date images whereas NDVIs is a 10 days composite data. In addition, the difference in the time step of aggregation of fluxes (10 days for NDVIs and 5 days for Landsat vegetation indices) rendered a comparison inappropriate. However, it should be noted that the highest correlation coefficient obtained with NDVIs is generally lower than the one obtained with Landsat vegetation indices. This is probably due to the greater variability in fluxes and NDVIs within the timeframe considered for the NDVIs data (10 days).

The use of the regression models in our study for mapping GPP or NEE seems interesting as it helped to appreciate the spatial distribution of carbon fluxes. However, the spatial variability in carbon fluxes only depended on the spatial variability of the vegetation indices. The obtained models should therefore be used only in homogenous environmental conditions.

During drought periods, an ecosystem can quickly shift from carbon sink to source (Lei et al., 2016). The difference observed in the maps of NEE between the greening and the dry phases illustrates this fact, since NEE values became positive during the dry phase, demonstrating the importance of comparing maps of the same area over time.

In the approach adopted in this study, VPD values from the eddy covariance tower are still needed to identify the greening and dry phases for a given date. This need of VPD in order to choose which model to apply could hinder the applicability over large areas where VPD values may change significantly. The possibility to retrieve VPD from meteorological stations could be explored in that case.

Another limitation of our study is the fact that there was no validation of the regression models. This is due the limited number of Landsat 8 images available along with missing flux data, not permitting to spare some data for validation. However, we consider that the model selection based on the good correlations observed and the regression accuracy metrics was robust enough and indicative of the utility of empirical regressions.

6. Conclusion

This study was particularly interesting, as it investigated the ability of several vegetation indices from two different remote sources in estimating carbon fluxes. It was equally compelling because it was conducted in a karst grassland, which is a particular ecosystem due to the rocky nature of the bedrock, and its relatively shallow soils.

The eddy covariance method represents a suitable method for measuring gas fluxes, which is widely used to assess and monitor the atmosphere-ecosystem carbon exchange. The fact that its measurements are limited to a relatively small footprint was addressed in this study, by attempting to estimate GPP and NEE for a homogenous area larger than the tower footprint. GPP showed some patterns of seasonality with two peaks, one at the end of May and another in October. In between the two peaks, a period of

low GPP was identified, which we later called dry phase while the rest of the growing season was referred to as greening phase. VPD was used to distinguish between the two phases, with the threshold of 1500 Pa above which begins the dry phase. Spectral vegetation indices from two sources (Landsat and SPOT-Vegetation) were explored, to test their ability as predictors in the estimation of NEE and GPP.

The main results of our study are the followings:

- ✓ A strong relationship was found between most of the vegetation indices and also between NEE and GPP, explaining the comparable performance of some of the regression models.
- ✓ NDVI proved to be the best predictor of GPP and NEE during the greening phase as the carbon uptake during that phase is mostly explained by changes in the green biomass in the plants. For the dry phase however, water-related vegetation indices such as LSWI and MNDWI were the best predictors of GPP and NEE, since they are more sensitive to drought.
- ✓ Good results were obtained not only for midday but also for daily (24 hours) fluxes, which is interesting since they could be more useful in terms of monitoring the carbon balance of an ecosystem, instead of considering only midday fluxes.
- ✓ Model type 1 (direct correlation between fluxes and vegetation indices) was the best for estimating midday average fluxes (GPP and NEE) and daily average of NEE whereas the models types 2 (direct correlation between fluxes and the product of PAR and vegetation indices) and 3 (simplified LUE model) were the best for daily average GPP.
- ✓ The maps of GPP and NEE could help appreciate spatial and temporal variability of fluxes. The two sources of NDVI data gave similar maps, in most of the cases. In those cases, the maps derived from NDVIs appeared as a generalization of maps derived from Landsat NDVI due to a lower spatial resolution of SPOT-Vegetation data. Following the spatial detail, the range of GPP and NEE values in the maps derived from Landsat is wider than the range of GPP and NEE derived from SPOT-Vegetation.

The results of this study seemed quite interesting, and the best regression models could be used for estimating carbon fluxes outside of the eddy covariance tower. Suggestions for further studies would be the validation of the models once more data would be available. The availability of Sentinel 2 images could also be considered. Alternatively, Landsat 7 images could be explored in order to use all the available eddy covariance data prior to 2014.

References:

Arnone III, J. A., Verburg, P. S. J., Johnson, D. W., Larsen, J. D., Jasoni, R. L., Lucchesi, A. J., … Schimel, D. S. (2008). Prolonged suppression of ecosystem carbon dioxide uptake after an anomalously warm year. *Nature*, *455*(7211), 383–386.

Aubinet, M., Vesala, T., and Papale, D. (2012). *Eddy Covariance A Practical Guide to Measurement and Data Analysis*-. Springer.

Bagnara, M., Van Oijen, M., Cameron, D., Gianelle, D., Magnani, F., and Sottocornola, M. (2018). Bayesian calibration of simple forest models with multiplicative mathematical structure: A case study with two Light Use Efficiency models in an alpine forest. *Ecological Modelling*, *371*, 90–100.

Bajgain, R., Xiao, X., Wagle, P., Basara, J., and Zhou, Y. (2015). Sensitivity analysis of vegetation indices to drought over two tallgrass prairie sites. *ISPRS Journal of Photogrammetry and Remote Sensing*, *108*, 151–160.

Baldocchi, D. D. (2008). "Breathing" of the terrestrial biosphere: lessons learned from a global network of carbon dioxide flux measurement systems. *Australian Journal of Botany*, *56*(1), 1.

Baldocchi, D. D., Hincks, B. B., and Meyers, T. P. (1988). Measuring Biosphere-Atmosphere Exchanges of Biologically Related Gases with Micrometeorological Methods. *Ecology*, *69*(5), 1331–1340.

Baldocchi, D. D., Sturtevant, C., and Fluxnet contributors. (2015). Does day and night sampling reduce spurious correlation between canopy photosynthesis and ecosystem respiration? *Agricultural and Forest Meteorology*, *207*, 117–126.

Benjamin, K., Domon, G., and Bouchard, A. (2005). Vegetation Composition and Succession of Abandoned Farmland: Effects of Ecological, Historical and Spatial Factors. *Landscape Ecology*, *20*(6), 627–647.

Bond-Lamberty, B., Wang, C., and Gower, S. T. (2004). A global relationship between the heterotrophic and autotrophic components of soil respiration? *Global Change Biology*, *10*(10), 1756–1766.

Burba, G., and Anderson, D. (2010). *A Brief Practical Guide to Eddy Covariance Flux Measurements: Principles and Workflow Examples for Scientific and Industrial Applications*. *LI-COR Biosciences*.

Buringh, P. (1984). Organic Carbon in Soils of the World. In G. M. Woodwell (Ed.), *The role of Terrestrial Vegetation in the Global Carbon Cycle: Measurement by Remote Sensing* (pp. 41 – 109). Chichester: SCOPE 23. Wiley.

CGLSP. (2017). Copernicus Global Land Service Portal. Retrieved December 20, 2017, from http://land.copernicus.vgt.vito.be/PDF/portal/Application.html#Browse;Root=513186;Collection=1000063;Time=NORMAL,NORMAL,-1,,,-1,,

Chavez, P. S. J. (1996). Image-based atmospheric corrections - revisited and improved. *Photogrammetric Engineering and Remote Sensing*, *62*(9), 1025–1036.

Desjardins, R. L. (1974). A technique to measure CO2 exchange under field conditions. *International Journal of Biometeorology*, *18*(1), 76–83.

EARS. (2018). Environmental Agency of the Republic of Slovenia. Retrieved from http://meteo.arso.gov.si

Ferlan, M. (2013). *The use of micro-meteorological methods for the monitoring of the carbon fluxes in karst ecosystems*. University of Ljubljana.

Ferlan, M., Alberti, G., Eler, K., Batič, F., Miglietta, F., Zaldei, A., and Simončič, P. (2011). Comparing carbon fluxes between different stages of secondary succession of a karst grassland. *Agriculture , Ecosystems and Environment*, *140*, 199–207.

Ferlan, M., Eler, K., Simončič, P., Batič, F., and Vodnik, D. (2016). Carbon and water flux patterns of a drought-prone mid-succession ecosystem developed on abandoned karst grasslan d. *Agriculture,*

Ecosystems and Environment, *20*, 152–163.

Gamon, J. A. (2015). Reviews and Syntheses: optical sampling of the flux tower footprint. *Biogeosciences*, *12*, 4509–4523.

Gamon, J. A., Field, C. B., Goulden, M. L., Griffin, K. L., Hartley, A. E., Joel, G., … Valentini, R. (1995). Relationships Between NDVI, Canopy Structure, and Photosynthesis in Three Californian Vegetation Types. *Ecological Applications*, *5*(1), 28–41.

Gilmanov, T., Soussana, J. F., Aires, L., Allard, V., Ammann, C., Balzarolo, M., … Wohlfahrt, G. (2007). Partitioning European grassland net ecosystem CO2 exchange into gross primary productivity and ecosystem respiration using light response function analysis. *Agriculture, Ecosystems & Environment*, *121*(1–2), 93–120.

Gilmanov, T., Tieszen, L. L., Wylie, B. K., Flanagan, L. B., Frank, A. B., Haferkamp, M. R., … Morgan, J. A. (2005). Integration of CO2 flux and remotely-sensed data for primary production and ecosystem respiration analyses in the Northern Great Plains: Potential for quantitative spatial extrapolation. *Global Ecology and Biogeography*, *14*(3), 271–292.

Gitelson, A. A., Kaufman, Y. J., and Merzlyak, M. N. (1996). Use of a green channel in remote sensing of global vegetation from EOS-MODIS. *Remote Sensing of Environment*, *58*(3), 289–298.

Gitelson, A. A., Viña, A., Verma, S. B., Rundquist, D. C., Arkebauer, T. J., Keydan, G., … Suyker, A. E. (2006). Relationship between gross primary production and chlorophyll content in crops: Implications for the synoptic monitoring of vegetation productivity. *Journal of Geophysical Research Atmospheres*, *111*(8).

Göckede, M., Foken, T., Aubinet, M., Aurela, M., Banza, J., Bernhofer, C., … Koebl, D. (2008). Quality control of CarboEurope flux data – Part 1 : Coupling footprint analyses with flux data quality assessment to evaluate sites in forest ecosystems. *Biogeosciences*, *5*, 433–450.

Goerner, A., Reichstein, M., Tomelleri, E., Hanan, N., Rambal, S., Papale, D., … Schmullius, C. (2011). Remote sensing of ecosystem light use efficiency with MODIS-based PRI. *Biogeosciences*, *8*, 189–202.

Griffis, T. J., Rouse, W. R., and Waddington, J. M. (2000). Interannual variability of net ecosystem CO2 exchange at a subarctic fen. *Global Biogeochemical Cycles*, *14*(4), 1109–1121.

Hall, D. O., Ojima, D. S., Parton, W. J., and Scurlock, J. M. O. (1995). Response of Temperate and Tropical Grasslands to CO 2 and Climate Change. *Journal of Biogeography*, *22*(2/3), 537.

Hall, D. O., and Scurlock, J. M. O. (1991). Climate Change and Productivity of Natural Grasslands. *Annals of Botany*, *67*(supp1), 49–55.

Hanson, P. J., Edwards, N. T., Garten, C. T., and Andrews, J. A. (2000). Separating root and soil microbial contributions to soil respiration: A review of methods and observations. *Biogeochemistry*, *48*(1), 115–146.

Haszpra, L., Barcza, Z., Davis, K. J., and Tarczay, K. (2005). Long-term tall tower carbon dioxide flux monitoring over an area of mixed vegetation. *Agricultural and Forest Meteorology*, *132*(1–2), 58–77.

Hill, M. J. (2013). Vegetation index suites as indicators of vegetation state in grassland and savanna: An analysis with simulated SENTINEL 2 data for a North American transect. *Remote Sensing of Environment*, *137*, 94–111.

Huete, A., Didan, K., Miura, T., Rodriguez, E. P., Gao, X., and Ferreira, L. G. (2002). Overview of the radiometric and biophysical performance of the MODIS vegetation indices. *Remote Sensing of Environment*, *83*(1–2), 195–213.

Huete, A. R. (1988). A soil-adjusted vegetation index (SAVI). *Remote Sensing of Environment*, *25*(3), 295–309.

Hui, D., Luo, Y., and Katul, G. (2003). Partition interannual variability in net ecosystem exchange between climatic variability and functional change. *Tree Physiology*, *23*, 433–442.

John, R., Chen, J., Lu, N., Guo, K., Liang, C., Wei, Y., … Han, X. (2008). Predicting plant diversity

based on remote sensing products in the semi-arid region of Inner Mongolia. *Remote Sensing of Environment*, *112*(5), 2018–2032.

Jovanović, D., Govedarica, M., Sabo, F., Važić, R., and Popović, D. (2016). Impact analysis of pansharpening Landsat ETM+, Landsat OLI, WorldView-2, and Ikonos images on vegetation indices. In K. Themistocleous, D. G. Hadjimitsis, S. Michaelides, & G. Papadavid (Eds.), *Fourth International Conference on Remote Sensing and Geoinformation of the Environment (RSCy2016)* (Vol. 9688, p. 10).

Kaligarič, M., Culiberg, M., and Kramberger, B. (2006). Recent vegetation history of the North Adriatic grasslands: Expansion and decay of an anthropogenic habitat. *Folia Geobotanica*, *41*, 241–258.

Keeley, J. E., and Keeley, S. C. (1984). Postfire Recovery of California Coastal Sage Scrub. *Source: The American Midland Naturalist*, *111*(1), 105–117.

Kirschbaum, M. U. F., Eamus, D., Gifford, R. M., Roxburgh, S. H., and Sands, P. J. (2001). Definitions Of Some Ecological Terms Commonly Used In Carbon Accounting. In *Net Ecosystem Exchange* (pp. 1–144).

Knez, M., Petrič, M., Slabe, T., and Šebela, S. (2015). *The Beka-Ocizla Cave System : karstological railway planning in Slovenia*. Springer International Publishing.

Lasslop, G., Reichstein, M., Detto, M., Richardson, A. D., and Baldocchi, D. D. (2010). Comment on Vickers et al.: Self-correlation between assimilation and respiration resulting from flux partitioning of eddy-covariance CO 2 fluxes. *Agricultural and Forest Meteorology*, *150*, 312–314.

Lasslop, G., Reichstein, M., Papale, D., Richardson, A. D., Arneth, A., Barr, A., … Wohlfahrt, G. (2010). Separation of net ecosystem exchange into assimilation and respiration using a light response curve approach: critical issues and global evaluation. *Global Change Biology*, *16*(1), 187–208.

Lees, K. J., Quaife, T., Artz, R. R. E., Khomik, M., and Clark, J. M. (2018). Potential for using remote sensing to estimate carbon fluxes across northern peatlands – A review. *Science of The Total Environment*, *615*, 857–874.

Lei, T., Pang, Z., Wang, X., Li, L., Fu, J., Kan, G., … Shao, C. (2016). Drought and Carbon Cycling of Grassland Ecosystems under Global Change: A Review. *Water*, *8*(10), 460.

Li, Y.-L., Tenhunen, J., Owen, K., Schmitt, M., Bahn, M., Droesler, M., … Bernhofer, C. (2008). Patterns in CO2 gas exchange capacity of grassland ecosystems in the Alps. *Agricultural and Forest Meteorology*, *148*(1), 51–68.

Li, Z., and Guo, X. (2018). Non-photosynthetic vegetation biomass estimation in semiarid Canadian mixed grasslands using ground hyperspectral data, Landsat 8 OLI, and Sentinel-2 images. *International Journal of Remote Sensing*, 1–21.

Li, Z., Yu, G., Xiao, X., Li, Y., Zhao, X., Ren, C., … Fu, Y. (2007). Modeling gross primary production of alpine ecosystems in the Tibetan Plateau using MODIS images and climate data. *Remote Sensing of Environment*, *107*(3), 510–519.

Lillesand, T. M., Kiefer, R. W., and Chipman, J. W. (2004). *Remote Sensing and Image Interpretation*. *Wiley*. WILEY.

Lobell, D. B., Asner, G. P., Ortiz-Monasterio, J. I., and Benning, T. L. (2003). Remote sensing of regional crop production in the Yaqui Valley, Mexico: estimates and uncertainties. *Agriculture, Ecosystems & Environment*, *94*(2), 205–220.

Ma, S., Baldocchi, D. D., Wolf, S., and Verfaillie, J. (2016). Slow ecosystem responses conditionally regulate annual carbon balance over 15 years in Californian oak-grass savanna. *Agricultural and Forest Meteorology*, *228–229*, 252–264.

Mäkelä, A., Pulkkinen, M., Kolari, P., Lagergren, F., Berbigier, P., Lindroth, A., … Hari, P. (2007). Developing an empirical model of stand GPP with the LUE approach: analysis of eddy covariance data at five contrasting conifer sites in Europe. *Global Change Biology*, *14*, 92–108.

Mason, J. A., and Zanner, C. W. (2005). GRASSLAND SOILS. In *Encyclopedia of Soils in the*

Environment (pp. 138–145). Elsevier.

Meyers, T. P. (2001). A comparison of summertime water and CO2 fluxes over rangeland for well watered and drought conditions. *Agricultural and Forest Meteorology*, *106*(3), 205–214.

Myneni, R. B., Hall, F. G., Sellers, P. J., and Marshak, A. L. (1995). The interpretation of spectral vegetation indexes. *Article in IEEE Transactions on Geoscience and Remote Sensing*, *33*(2), 481–486.

Myneni, R. B., and Williams, D. L. (1994). On the relationship between FAPAR and NDVI. *Remote Sensing of Environment*, *49*(3), 200–211.

Nestola, E., Calfapietra, C., Emmerton, C. A., Wong, C. Y. S., Thayer, D. R., and Gamon, J. A. (2016). Monitoring grassland seasonal carbon dynamics, by integrating MODIS NDVI, proximal optical sampling, and eddy covariance measurements. *Remote Sensing*, *8*(3), 25.

Pan, Y., Birdsey, R. A., Fang, J., Houghton, R., Kauppi, P. E., Kurz, W. A., … Hayes, D. (2011). A Large and Persistent Carbon Sink in the World's Forests. *Science*, *333*(6045), 988–993.

Papale, D., Reichstein, M., Aubinet, M., Canfora, E., Bernhofer, C., Kutsch, W., … Yakir, D. (2006). Towards a standardized processing of Net Ecosystem Exchange measured with eddy covariance technique: algorithms and uncertainty estimation. *Biogeosciences*, *3*, 571–583.

Peichl, M., Carton, O., and Kiely, G. (2012). Management and climate effects on carbon dioxide and energy exchanges in a maritime grassland. *Agriculture, Ecosystems & Environment*, *158*, 132–146.

Post, W. M., and Kwon, K. C. (2000). Soil carbon sequestration and land-use change : processes and potential. *Global Change Biology*, *6*, 317–327.

Reichstein, M., Falge, E., Baldocchi, D. D., Papale, D., Aubinet, M., Berbigier, P., … Valentini, R. (2005). On the separation of net ecosystem exchange into assimilation and ecosystem respiration: review and improved algorithm. *Global Change Biology*, *11*(9), 1424–1439.

Rocha, A. V., and Shaver, G. R. (2009). Advantages of a two band EVI calculated from solar and photosynthetically active radiation fluxes. *Agricultural and Forest Meteorology*, *149*(9), 1560–1563.

Rodriguez-Iturbe, I., Porporato, A., Laio, F., and Ridolfi, L. (2001). Intensive or extensive use of soil moisture: Plant strategies to cope with stochastic water availability. *Geophysical Research Letters*, *28*(23), 4495–4497.

Rossini, M., Cogliati, S., Meroni, M., Migliavacca, M., Galvagno, M., Busetto, L., … Colombo, R. (2012). Remote sensing-based estimation of gross primary production in a subalpine grassland. *Biogeosciences*, *9*, 2565–2584.

Rouse, J. W., Haas, R. H., Schell, J. A., and Deering, D. W. (1974). Monitoring vegetation systems in the Great Plains with ERTS. In *Proceedings, 3rd Earth Resources Satellite-1 Symposium (NASA SP-351)*. Maryland.

Ruimy, A., Jarvis, P. G., Baldocchi, D. D., and Saugier, B. (1995). CO2 Fluxes over Plant Canopies and Solar Radiation: A Review. In *Advances in Ecological Research* (pp. 1–68).

Running, S. W., Nemani, R. R., Heinsch, F. A., Zhao, M., Reeves, M., and Hashimoto, H. (2004). A Continuous Satellite-Derived Measure of Global Terrestrial Primary Production. *BioScience*, *54*(6), 547.

Saigusa, N., Yamamoto, S., Murayama, S., Kondo, H., and Nishimura, N. (2002). Gross primary production and net ecosystem exchange of a cool-temperate deciduous forest estimated by the eddy covariance method. *Agricultural and Forest Meteorology*, *112*, 203–215.

Saranya, M. (2014). Cloud Removal from Satellite Images Using Information Cloning. *International Journal of Computer Science and Mobile Computing*, *32*(2), 681–688.

Scurlock, J. M. O., and Hall, D. O. (1998). The global carbon sink: a grassland perspective. *Global Change Biology*, *4*(2), 229–233.

Sonmez, N. K., and Slater, B. (2016). European Journal of Remote Sensing Measuring Intensity of

Tillage and Plant Residue Cover Using Remote Sensing. *European Journal of Remote Sensing*, *49*, 121–135.

Sun, L., Mi, X., Wei, J., Wang, J., Tian, X., Yu, H., and Gan, P. (2017). A cloud detection algorithm-generating method for remote sensing data at visible to short-wave infrared wavelengths. *ISPRS Journal of Photogrammetry and Remote Sensing*, *124*, 70–88.

USGS. (2018). United States Geological Survey. Retrieved January 5, 2018, from https://glovis.usgs.gov/

Xiao, X., Boles, S., Liu, J., Zhuang, D., Frolking, S., Li, C., … Moore, B. (2005). Mapping paddy rice agriculture in southern China using multi-temporal MODIS images. *Remote Sensing of Environment*, *95*(4), 480–492.

Xu, H. (2006). Modification of normalised difference water index (NDWI) to enhance open water features in remotely sensed imagery. *International Journal of Remote Sensing*, *27*(14), 3025–3033.

Yan, W., Hu, Z., Zhao, Y., Zhang, X., Fan, Y., and Shi, P. (2015). Modeling Net Ecosystem Carbon Exchange of Alpine Grasslands with a Satellite-Driven Model. *PLoS ONE*, *10*(4), 1–16.

Yao, Y., Li, Z., Wang, T., Chen, A., Wang, X., Du, M., … Piao, S. (2018). A new estimation of China's net ecosystem productivity based on eddy covariance measurements and a model tree ensemble approach. *Agricultural and Forest Meteorology*, *253–254*, 84–93.

Yuan, W., Cai, W., Xia, J., Chen, J., Liu, S., Dong, W., … Wohlfahrt, G. (2014). Global comparison of light use efficiency models for simulating terrestrial vegetation gross primary production based on the LaThuile database. *Agricultural and Forest Meteorology*, *192–193*, 108–120.

Zhou, X., Zhu, Q., Tang, S., Chen, X., and Wu, M. (2002). Interception of PAR and relationship between FPAR and LAI in summer maize canopy. In *International Geoscience and Remote Sensing Symposium* (Vol. 6, pp. 3252–3254). IEEE.

Zhou, Y., Zhang, L., Xiao, J., Chen, S., Kato, T., and Zhou, G. (2014). A comparison of satellite-derived vegetation indices for approximating gross primary productivity of grasslands. *Rangeland Ecology and Management*, *67*(1), 9–18.